The Canadian Mineralogist
Vol. 46, pp. 1207-1213 (2008)
DOI: 10.3749/canmin.46.5.1207

THE HIGH-TEMPERATURE BEHAVIOR OF CHAROITE

EMILIO MATESANZ

Centro de Apoyo a la Investigacion de DRX, Universidad Complutense Madrid, E–28040 Madrid, Spain

JAVIER GARCIA-GUINEA AND ELENA CRESPO-FEO

Museo Nacional Ciencias Naturales, Jose Gutierrez Abascal 2, E–28006 Madrid, Spain

PAULA LOPEZ-ARCE

Getty Conservation Institute, 1200 Getty Center Drive, Suite 700, Los Angeles, California 90049, U.S.A.

FRANCISCO J. VALLE-FUENTES

Instituto de Cerámica y Vidrio, CSIC. Cantoblanco, E–28049 Madrid, Spain

VIRGILIO CORRECHER§

CIEMAT, Avenida Complutense 22, E–28040 Madrid, Spain

ABSTRACT

The effect of thermal annealing on charoite, $K_5 Ca_8 (Si_6O_{15}) (Si_2O_7) (Si_4O_9) (OH)\bullet 3H_2O$, have been studied by X-ray diffraction (XRD), differential thermal analysis (DTA), thermogravimetry (TG) and thermoluminescence (TL). The chemical composition, established by electron-probe micro-analysis (EPMA), indicates significant amounts of Na, Ba, Fe and F; the environmental scanning electron microscope (ESEM) results reveal the presence of unusual minerals such as tinaksite and aegirine. The cell parameters of both natural and preheated charoite, determined by XRD, are (i) *a* 19.786(2), *b* 32.003(3), *c* 7.8565(9) Å, α 90, β 97.159, γ 90°, with a F(30) of 43 for the non-annealed sample, and (ii) *a* 19.567(2), *b* 31.821(3), *c* 7.1171(7) Å, α 90, β 94.000(2), γ 90°, with a F(30) of 19 for charoite heated to 710°C. The thermal effect indicates a shortening of the cell edges, Δ*a* 0.219(2), Δ*b* 0.182, Δ*c* 0.739 Å, and the β angle tilts only by 3.16°. The DTA–TG and TL emission suggest: (i) a thermal interval of 80°–290°C, explained by the dehydration of charoite, involving different types of H_2O, *i.e.*, hydrogen-bonded to the framework and non-bonded H_2O, and (ii) an interval 290°–480°C, resulting from a dehydroxylation process.

Keywords: charoite, structure, dehydration, X-ray diffraction, differential thermal analysis, thermogravimetry, thermoluminescence.

SOMMAIRE

Le produit d'un recuit thermique de la charoïte, $K_5 Ca_8 (Si_6O_{15}) (Si_2O_7) (Si_4O_9) (OH)\bullet 3H_2O$, a été étudié par diffraction X (XRD), analyse thermique différentielle (DTA), thermogravimétrie (TG) et thermoluminescence (TL). La composition chimique, établie avec une microsonde électronique, indique des quantités non négligeables de Na, Ba, Fe et F; le microscope électronique à balayage environnemental révèle la présence de minéraux inhabituels comme la tinaksite et l'aegyrine. Les paramètres réticulaires de la charoïte à l'état naturel et chauffée, déterminés par diffraction X, sont: (i) *a* 19.786(2), *b* 32.003(3), *c* 7.8565(9) Å, α 90, β 97.159, γ 90°, avec une valeur de F(30) de 49 pour l'échantillon naturel, et (ii) *a* 19.567(2), *b* 31.821(3), *c* 7.1171(7) Å, α 90, β 94.000(2), γ 90°, avec une une valeur de F(30) de 19 pour la charoïte chauffée jusqu'à 710°C. Le réchauffement cause un raccourcissement des dimensions de la maille, Δ*a* 0.219(2), Δ*b* 0.182, Δ*c* 0.739 Å, et l'angle β ne s'incline que par 3.16°. Les données obtenues par DTA–TG et l'émission TL semblent indiquer: (i) un intervalle thermique entre 80° et 290°C au cours duquel il y aurait déshydratation de la charoïte impliquant des différent types de H_2O, *i.e.*, H_2O fixé au réseau par liaisons hydrogène et H_2O moléculaire sans liaisons, et (ii) un intervalle entre 290° et 480°C, résultat d'un processus de déshydroxylation.

(Traduit par la Rédaction)

Mots-clés: charoïte, structure, déshydratation, diffraction X, analyse thermique différentielle, analyse thermique, thermogravimétrie, thermoluminescence.

§ *E-mail address*: v.correcher@ciemat.es

Introduction

Charoite forms at 200°–250°C by alteration of limestone in the presence of solutions emanating from the Murun nepheline syenite intrusion, one of the several Mesozoic potassic alkaline complexes located in the Aldan shield, in the southern part of Olekminsk, eastern Siberia, Russia (Mitchell *et al.* 1994). The Murun complex formed by magmatic evolution from an alkaline ultrabasic to basic, intermediate, to peralkaline granite and nepheline syenite by a long-term differentiation and vertical zonation of the alkaline magma (Vladykin 2000). The chemical formula of charoite varies among different outcrops, and it commonly possesses inclusions of aegirine, feldspar, tinaksite and some other rather uncommon minerals. The metasomatic rock also exhibits a complex association with unusual minerals such as charoite, canasite, fedorite, ekanite, miserite, tinaksite, benstonite, tokkoite, murunskite, frankamenite and davanite, together with other more common minerals such as pectolite, aegirine, microcline and quartz (Reguir 2001). Some the characteristic features of the crystal structures of these unusual minerals (canasite, frankamenite, miserite, tinaksite and tokkoite) have been reported by Rozhdestvenskaya & Nikishova (2002).

From a chemical point of view, charoite is an interesting phase as it contains large amounts of K, Na, Ca, Ba, Sr, Br and F. This open lattice holds very different cations and is highly resistant to thermal dehydration, though there are few investigations of thermal effects on charoite samples. To the best of our knowledge, only Kraeff *et al.* (1980) performed differential thermogravimetric analyses (DTA) of charoite and showed two main steps, *ca.* 290° and 430°C, associated with the dehydration process. What is well known about this mineral is that there is (i) no aluminum (0.01%), (ii) only a small amount of sodium (2%), (iii) hydroxyl groups, (iv) coexistence of large amounts of potassium (9.5%) and calcium (22%), and (v) a purple color attributed to 0.1% of MnO and 0.01% of Fe_2O_3. Reguir (2001) suggested that Mn^{2+} and Mn^{3+} ions are responsible for the color and luminescence emission of charoite. Charoite is a rare species, probably owing to the specific chemical reaction between a limestone and an alkaline fluid subjected to unusual physical conditions of the massif. The color of charoite is described as a stunning purple forming a swirling pattern of interlocking fibers. The International Mineralogical Association approved it as a new mineral in 1978, with the formula $K_5Ca_8(Si_6O_{15})(Si_2O_7)(Si_4O_9)(OH)\bullet 3H_2O$ (Rogova *et al.* 1978). It is included in the Dana classification class 70.1.2.3 as chain-silicate with a column or tube structure, with columnar silicate units of double crankshaft chains, *i.e.*, monoclinic *P**/4 (pseudo-orthorhombic) 2/*m*. However, according to the publications on charoite, there is no agreement concerning the unit-cell parameters (Rogova *et al.* 1978, Nikishova *et al.* 1984).

In this work, we focus on the thermal study of a well-characterized sample of charoite. To this end, we employ (i) *in situ* high-temperature X-ray diffraction (HTXRD), (ii) simultaneous thermal-differential thermal analysis and thermogravimetry (DTA–TG), and (iii) thermoluminescence (TL) of natural aliquots of representative chips of charoite.

Samples, Experimental and Analytical Techniques

Charoite samples were selected from sets of high-quality gemstones from Murun massif. The color of the charoite masses is intense purple, and the material forms a swirling pattern of interlocking crystals. It shows strong anisotropy with white (K-feldspar-bearing) and black (aegirine-bearing) areas mixed in with the charoite. Analytical samples for the thermal measurements were chosen from the purple areas of coarse micro-folds (Fig. 1a). The morphology and composition of charoite crystals, and of the associated less common minerals, were assessed under environmental scanning electron microscopy and energy-dispersive X-ray spectroscopy using a Philips XL30/40 EDS–ESEM (Fig. 1b). Polished specimens of charoite were coated with graphite (20 nm) in a Bio-Rad SC515 sputter coating unit. The chemical composition of the charoite specimens (electron-microprobe analysis) is 58.5% SiO_2, 0.03% Al_2O_3, 0.14% Fe_2O_3, 0.1% MnO, 2.53% BaO, 21.9% CaO, 2.26 Na_2O, 10.01% K_2O, 0.02% TiO_2, 0.03% P_2O_5, 0.33% F_2, 0.02% Cl_2 and 4.13% Loss on Ignition. These measurements were performed with a Jeol Superprobe JXA–8900M instrument, with bulk and channel-selected (TAP, PETJ, LIF, PETH) X-ray spectra. Natural standards and synthetic crystals from the collection of the "Servicio de Microscopia Electronica Luis Bru", Complutense University have been used for this purpose.

The powder pattern of the minerals was acquired with a Panalytical X'Pert PRO Alpha1 diffractometer equipped with a Ge primary-beam monochromator and a X'Celerator fast detector (Cu$K\alpha$ radiation, 45 kV, 40 mA). Patterns were obtained by continuous scanning from 1.5° to 70°2θ in steps of 0.017°. Conditions of maximum resolution were used: intensity loss was compensated with long counting-times. The effective counting-time per step was 1725 s for charoite, and 3562 s for 710°C-preheated charoite. High-temperature powder X-ray-diffraction patterns were recorded between room temperature (RT) and 710°C using a Panalytical X-Pert PRO MPD diffractometer (Cu$K\alpha$ radiation, 45 kV, 40 mA) equipped with a high-temperature Anton Paar HTK1200 camera and a X'Celerator fast detector with a Ni β filter. The isothermal runs from 2° to 50° 2θ were measured at different *in situ* temperatures, from RT to 710°C (varying intervals of 20°C and then back to RT after heating), with a scan step-size of 0.034° 2θ and a time per step of 49.3 s. The

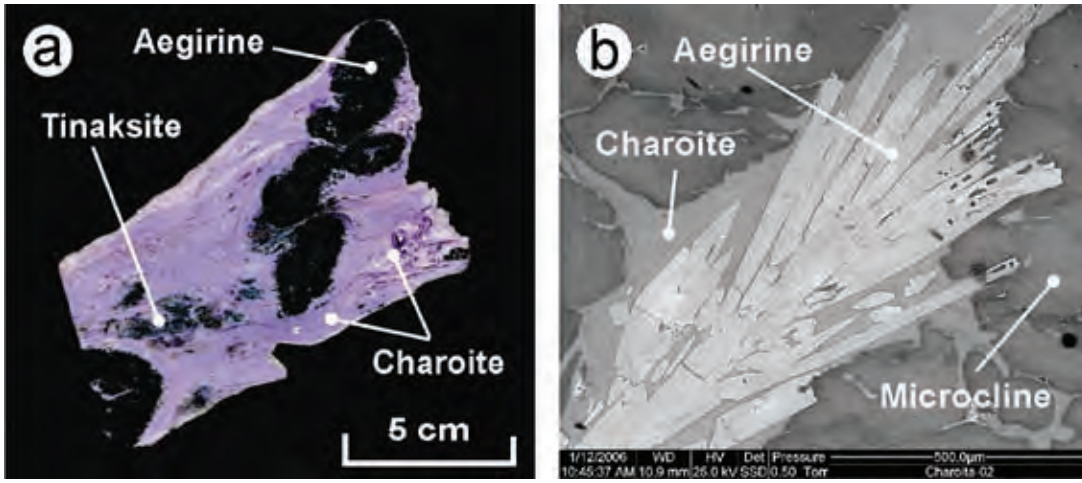

FIG. 1. (a) Charoite-bearing specimen with black masses of aegirine and yellow spots of tinaksite; (b) SEM image with aegirine crystals, charoite masses and K-feldspar.

heating rate was 5°C·min^{-1} and an additional delay of 2 min was introduced before scanning to facilitate the stabilization of the temperature. Samples were mounted on a standard alumina sample-holder for this camera (circular sample-holder with a cavity of 0.8 mm for front loading). The temperature was measured using a Pt–10% RhPt thermocouple. All experiments were carried out in air.

Thermogravimetric and differential thermal analysis (TG–DTA) of 50.6 mg of sample was recorded with a simultaneous TG–DTA–DSC thermal analyzer (Setaram, Labsys CS 32–CS 332 Controller) also in air. Thermal treatments were performed with a first gradient at a heating rate of 20°C·min^{-1} from RT up to 80°C, a second ramp at 10°C·min^{-1} up to 1000°C, and an isothermal treatment for 5 minutes at this last temperature. The sample was packed in an alumina crucible, and the reference material was an empty alumina crucible. The thermoluminescence measurements on charoite were performed using an automated Risø system, model TL DA–12 (Bøtter-Jensen & Duller 1992). This reader is provided with an EMI 9635 QA photomultiplier, and the emission was observed through a blue filter (FIB002, Melles-Griot Company), with which the wavelength peaked at 320–480 nm. The full-width at half-maximum (FWHM) value is 80 ± 16 nm, and peak transmittance (minimum) is 60%. The TL reader is also provided with a ^{90}Sr/^{90}Y source with a dose rate of 0.020 Gy•s^{-1} calibrated against a ^{60}Co photon source, in a secondary standards laboratory (Correcher & Delgado 1998). All TL measurements were performed using a linear heating rate of 5°C•s^{-1} from RT up to 550°C, in a N_2 atmosphere. Several aliquots of 5.0 ± 0.1 mg of each sample of charoite were used for each measurement. The incandescent background was directly subtracted from the TL data. The sample was carefully powdered with an agate mortar and pestle to avoid triboluminescence (Garcia-Guinea & Correcher 2000).

DISCUSSION OF THE EXPERIMENTAL RESULTS

X-ray diffraction of charoite aliquots

The identification of charoite was performed with an experimental XRD diffractogram recorded very slowly using monochromatic radiation. The results obtained fit very well with the pattern ICDD 42–1402 and the results published by Rogova *et al*. (1978) and Fleischer (1978). However, several lines of our experimental diffractogram are not included in the ICDD file 42–1402, but could be also assigned to charoite (Fig. 2). Cell parameters of charoite aliquots, natural and preheated up to 710°C, were determined from diffractograms collected at low speed with Cu$K\alpha_1$ radiation and the best available resolution of the XRD equipment. The indexing of charoite diffraction patterns, cell parameters and the space-group test were performed using DICVOL04 (Boultif & Louër 2004) program, included in the X'Pert Highscore Plus v2.1b (Panalytical) sofware. It allows us to obtain the best explanation for the peak list based on the calculated Figure of Merit (FOM) of Snyder (Smith & Snyder 1979), and the number of missing or unexplained peaks.

The cell parameters were estimated taking into account the following sequence: (i) compare the list of the peaks in the ICDD 42–1402 pattern with the cell parameter reported, (ii) index the list of the peaks obtained from the sample studied here by refining the

cell parameters in the ICDD 42–1402 card, (iii) indexing our list of peaks with published unit-cell parameters of charoite, *i.e., a* 19.610, *b* 32.120, *c* 7.200 Å, α 90.000, β 93.760, γ 90.000° (Nikishova *et al*. 1984) and (iv) *ab initio* calculations.

Testing the ICDD 42–1402, we found good agreement between observed and calculated 2θ angles computed for Cu$K\alpha_1$ when compared with the proposed cell parameters, *i.e.,* $-0.1 < \delta 2\theta < +0.1$. The exception is the 11.35° peak (Fig. 2), which remains quite distant from the theoretical value; in accordance with this card-file, this peak is indexed as 040.

Using our experimental XRD data, the refinement of the ICDD 42–1402 cell displays a better FOM compared to the card data; we also observe how the 11.34° peak moves *ca*. 0.3°, away from the calculated value.

Using the XRD data for cell-1 proposed by Nikishova *et al*. (1984), we obtain similar cell parameters in comparison with those defined in the 42–1402 card; the 11.34° peak is also shifted. Conversely, using the cell-2 data proposed by those authors, many peaks are mismatched, providing an unacceptable solution.

The *ab initio* calculations using only our own results in DICVOL offer another unit-cell refinement with a better FOM, still close to the published data. Using DICVOL on the initial 40 peaks, a single result becomes apparent: *a* 19.786(2), *b* 32.003(3), *c* 7.8565(9), α 90, β 97.159(2), γ 90° with a value of F(30) of 0.43. We suggest these unit-cell parameters despite the fact that the small peak at 31.74° shifted 0.12° from the theoretical value.

The test of all the possible space-groups was estimated assuming that the indexing that yielded the best results using a primitive β-monoclinic cell. According to the FOM values, we determined that the more probable space-groups for charoite are *P*2, *Pm*, or *P*2/*m*, which agrees with the published choices (Nikishova *et al*. 1984).

Similarly, the preheated charoite aliquot at 710°C was analyzed by XRD at room temperature (Cu$K\alpha_1$ radiation). We propose the following parameters for

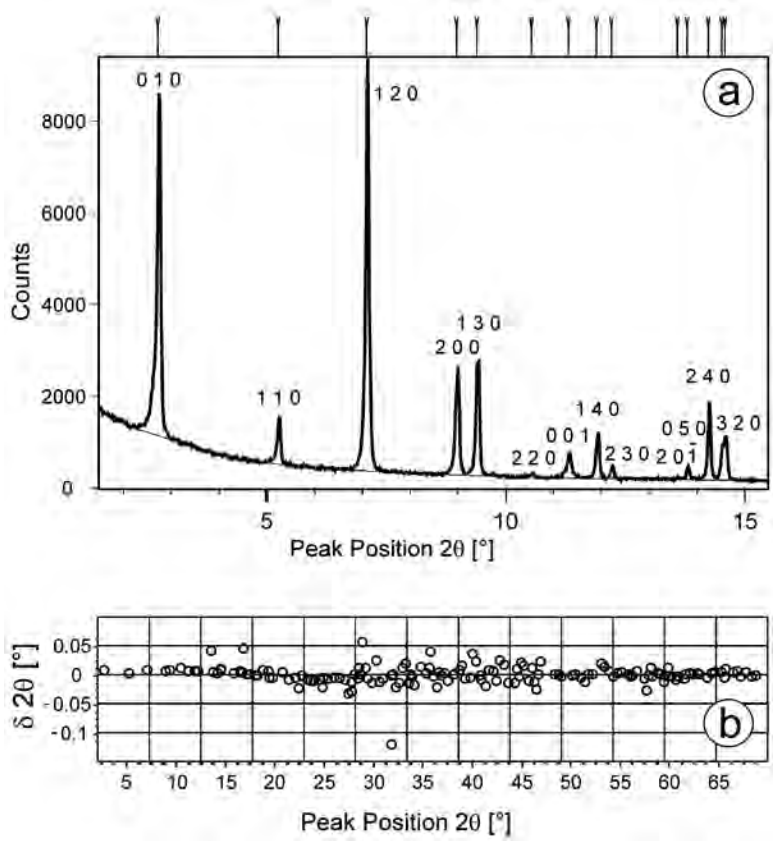

FIG. 2. (a) Indexation of the X-ray diffractogram of natural charoite taken at room temperature. (b) Plot δ2θ *versus* 2θ positions of this sample of charoite.

this anhydrous charoite: *a* 19.567(2), *b* 31.821(3), *c* 7.1171(7), α 90°, β 94.000°(2), γ 90°; F(30) = 19; space-groups *P*2, *Pm* or *P*2/*m*. In addition to the obvious dehydration–dehydroxylation of charoite as the sample was heated from room temperature to 710°C, the axes shortened, as shown by the irreversible thermal contraction of the charoite cell: Δ*a* 0.219, Δ*b* 0.182, Δ*c* 0.7394 Å. On the other hand, the angles α and γ remain orthogonal at 90°, and the β angle tilted by only 3.159°. The *in situ* thermal XRD profiles (Figs. 3a, b) reveal that the main crystallographic orientation (001) of charoite disappears at ~240°. In addition, for several peaks, the trend of the *d* value *versus* temperature changes at about 380°C, as shown in Figure 3b. This contraction of the charoite structure, from 240°C to 380°C, supposes a re-orientation of the crystals due to the thermal annealing that could be linked to dehydration–dehydroxylation processes.

TG–DTA and TL analyses

The endothermic peaks observed in the differential thermal analysis due to the heat absorption during dehydration and dehydroxylation processes agree with the coupled thermogravimetric analyses (Fig. 4). The first endothermic peak at ~40°C agrees with a first loss of mass due to the sample dehydration of absorbed H_2O. Although H_2O loss is continuous between temperatures from ~40 to ~500°C, three major steps can be distinguished at 210, 290 and 480°C (Fig. 4). We infer that the gap 80–290°C may reflect a dehydration of different types of H_2O, *i.e.,* hydrogen-bonded to the charoite lattice and non-bonded H_2O. Furthermore, the interval 290–480°C could imply a different solid-state process of H_2O losses, such as a dehydration–dehydroxylation step represented by the following features: (i) TG: changes in slope at 290 and 500°C, which could be interpreted as increasingly slow losses of H_2O or OH by various structural mechanisms, (ii) DTA endothermic peaks at 210, 290 and 480°C, *i.e.,* possible losses of H_2O, and a clear exothermic peak at ~360°C that can be explained by a reorientation of the crystals with the corresponding shortening of structural axes and slight modifications in the β angle, (iii) a TL glow curve peaked at ~250°C and ~360°C, which agrees with two crucial intervals of dehydration of possible hydrogen-bonded H_2O (~210–290°C) and with a possible dehydroxylation process (~290–480°C) (Fig. 4). The thermal XRD profiles of charoite show that the (001) peak vanishes at about ~240°C, in agreement with the TG–DTA and TL data. This observation supports the hypothesis of H_2O losses with stronger links to the charoite lattice, *e.g.,* hydrogen bonds.

In this sense, the use of the TL is of interest, as it supplies information, among others, on (i) trapped charge-recombination sites related to metastable defects inside the lattice (McKeever 1985), (ii) phase transitions (Correcher *et al.* 2004a), and (iii) consecutive breaking and linking of bonds including redox reactions, dehydroxylation and dehydration processes (Correcher *et al.* 2004b). This property is based on the emission of light from a dielectric solid sample (insulator or semiconductor) when it is heated after being exposed to ionizing radiation such as X-rays, gamma rays, beam of electrons, *etc.* (McKeever 1985). During the analytical heating, the TL signal is registered by a photomultiplier tube and recorded as a function of temperature or wavelength as a TL glow curve. The spectra of the minerals can be compared to characterize the emission bands that are associated with the presence of different impurities, *e.g.,* Mn ions giving rise to the green emission or Fe

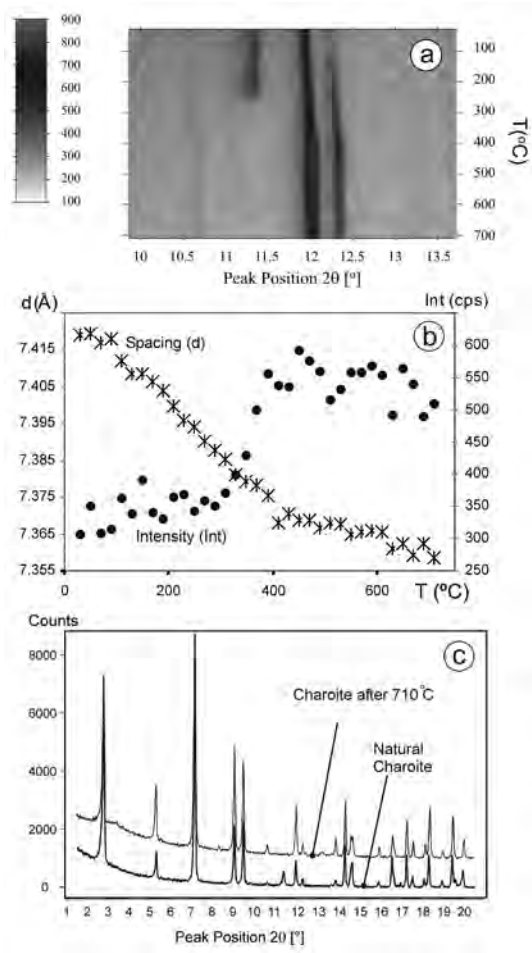

FIG. 3. (a) Contour plot depicting in detail the *in situ* diffractograms of charoite. Note the disappearance of the peak 11.2 (2θ) at *ca.* 240°C. (b) Plots of temperature *versus* spacing and *versus* intensity of the XRD (140) peak. (c) A comparative plot of both XRD diffractogram of the natural and 710°C preheated charoite.

centers producing the red waveband (Brooks *et al.* 2002, Finch *et al.* 2003, Garcia-Guinea *et al.* 1999). Luminescence techniques are also used to study the types and spatial distribution of point defects in natural minerals, *e.g.,* diamond, and detecting post-growth ionizing irradiation with further low-temperature annealing in natural conditions (Chakhmouradian *et al.* 2002).

The origin of the UV blue 380°C TL of charoite, with an intensity of 40,000 a.u. (arbitrary units), can be explained if the following assumptions are made. (i) Some orientations of the charoite structure undergo stress during the irreversible dehydration–dehydroxylation ending at 380°C. (ii) Charoite invariably displays a blue luminescence (Gorobets & Rogojine 2002). (iii) The 340 nm emission peak is very common in the luminescence spectra of silicates (silica, feldspars, feldspathoids, *etc.*) in which their 3D framework silicon–oxygen structures are stressed. These Si–O strained structures include some non-bridging oxygen (NBOC) atoms or silicon vacancy-hole centers and Si–O bonding defects, which seem to be responsible for this common 340 nm emission. One can therefore speculate that the charoite structure includes such centers. (iv) Many Si–O bonds undergo an additional stress due to different processes, namely dehydration or dehydroxylation or both, involving losses of H_2O, with hydrogen atoms bonded to the lattice, or the breaking of hydroxyl groups, also bonded to the silicate framework. (v) The charoite composition has silicon and cations such as K and Ca, but little Al; for this reason, we minimize the importance of $[AlO_4]$°–alkali centers producing the blue emission at ~400 nm. These processes, observed in other hydrolyzed minerals, are interpreted as being due to a continuum in the trap distribution or to the existence of a tunneling recombination process in coincidence with the dehydroxylation temperature of charoite (Correcher *et al.* 2008).

The mechanism that induces the 340 nm emission could be a combination of NBOC (generated from the surface charge of hydroxyl groups) and the vibrational absorption of a SiO_2 network containing H_2O (Yao *et al.* 2001). Anedda *et al.* (2003) could observe how the UV emission does not depend on the chemical composition of the samples but is related to the chemical and the physical states of the surfaces. They concluded that such emission increases significantly with the increase of OH groups adsorbed on the surface of porous silica.

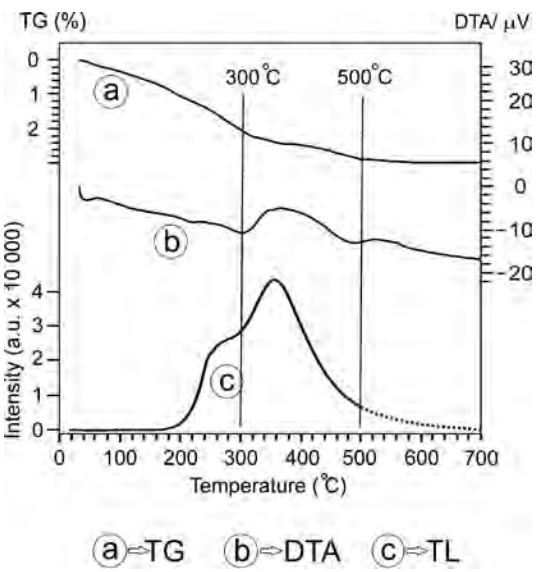

FIG. 4. (a) Thermogravimetric (TG), (b) differential thermal analysis (DTA) and (c) thermoluminescence (TL) response of natural (unheated) charoite.

CONCLUSIONS

1. The EPMA and ESEM analyses of the charoite masses display aegirine, tinaksite and microcline. Despite the complex paragenesis, we were able to extract grains of charoite with a reasonable purity and homogeneity. The behavior of the aliquots chemically studied under EPMA and structurally under XRD, DTA–TG and TL is quite consistent, *i.e.,* there are no significant deviations of the measurements.

2. The cell parameters of natural charoite have been determined by means of XRD using the initial 40 peaks. The estimated values are: *a* 19.786(2), *b* 32.003(3), *c* 7.8565(9) Å, α 90, β 97.159(2), γ 90°, with a F(30) value of 43. The small peak at 31.74° shifts 0.12° from the predicted position. Preheated charoite at 710°C was also analyzed by XRD at room temperature with Cu$K\alpha_1$ radiation, with the following results: *a* 19.567(2), *b* 31.821(3), *c* 7.1171(7) Å, α 90, β 94.000(2), γ 90°, with a F(30) value of 19. The thermal treatment of the charoite cell led to a shortening of axes: Δ*a* 0.219(2), Δ*b* 0.182, Δ*c* 0.7394 Å, whereas the angles α and γ remain orthogonal at 90°, and β angle tilts only 3.159°. Possible space-groups for both preheated and non-preheated charoite are *P*2, *Pm*, or *P*2/*m,* in good agreement with the literature.

3. On the basis of the TG–DTA analyses, (1) the gap 80°–290°C could be associated with charoite dehydration of different types of H_2O, *i.e.,* hydrogen-bonded to the charoite lattice and non-bonded H_2O groups, (2) the interval 290°–480°C could be linked to dehydroxylation processes. The TL glow curves display a maximum peak at 250°C and 360°C, which agree with two crucial intervals of dehydration of possible hydrogen-bonded H_2O (~210°–290°C) and with a possible dehydroxylation process (~250°–380°C). The high blue TL intensity of the sample is attributed to the strained structure of charoite, including possible non-bridging oxygen atoms, silicon vacancy-hole centers and Si–O bonding defects, which seem to be responsible for this common 340 nm emission in stressed silicates.

Acknowledgements

This work has been supported by CAM (06/0134/2003), MCYT (BQU2003–08531–C02–01); CICYT (FIS2007–61823) and Comunidad Autonoma de Madrid (CAM) MATERNAS–S–0505/MAT/0094 projects. Emilio Matesanz is working under a contract supported by the FSE by the Spanish MCyT. Thanks are also due to Martin Fernandez Hernan for the valuable help with the charoite samples provided. We acknowledge the constructive comments received from the referees and the editor.

References

Anedda, A., Carbonaro, C.M., Clemente, F., Corpino, R., Raga, F. & Serpi, A. (2003): Ultraviolet excitation of photoluminescence of porous silica under vacuum conditions. *J. Non-Cryst. Solids* **322**(1-3), 95-99.

Bøtter-Jensen, L. & Duller, G.A.T. (1992): A new system for measuring optically stimulated luminescence from quartz samples. *Nucl. Tracks Radiat. Meas., Part D* **20**, 549-553.

Boultif, A. & Louër, D. (2004): Powder pattern indexing with the dichotomy method. *J. Appl. Crystallogr.* **37**, 724-731.

Brooks, R.J., Finch, A.A., Hole, D.E., Townsend, P.D. & Wu, Zheng-Long (2002): The red to near-infrared luminescence in alkali feldspar. *Contrib. Mineral. Petrol.* **143**, 484-494.

Chakhmouradian, A.R., Reguir, E.P. & Mitchell, R.H. (2002): Strontium-apatite: new occurrences, and the extent of Sr-for-Ca substitution in apatite-group minerals. *Can. Mineral.* **40**, 121-136.

Correcher, V. & Delgado, A. (1998): On the use of natural quartz as transfer dosimeter in retrospective dosimetry. *Radiat. Meas.* **29**, 411-414.

Correcher, V., Garcia-Guinea, J., Lopez-Arce, P. & Gomez-Ros, J.M. (2004a): Luminescence emission spectra in the temperature range of the structural phase transitions of Na_2SO_4. *Spectrochim. Acta* **A60**, 1431-1438.

Correcher, V., Gomez-Ros, J.M., Garcia-Guinea, J. & Delgado, A. (2004b): Thermoluminescence kinetic parameters of basaltic rock samples due to continuous trap distribution. *Nucl. Instrum. Meth. A* **528**, 717-720.

Correcher, V., Gomez-Ros, J.M., Garcia-Guinea, J., Lis, M. & Sanchez-Muñoz, L. (2008): Calculation of the activation energy in a continuous trap distribution system of a charoite silicate using initial rise and TL glow curve fitting methods. *Radiat. Meas.* **43**, 269-272.

Finch, A.A., Hole, D.E. & Townsend, P.D. (2003): Orientation dependence of luminescence in plagioclase. *Phys. Chem. Minerals* **30**, 373-381.

Fleischer, M. (1978): New mineral names. *Am. Mineral.* **63**, 1289-1291.

Garcia-Guinea, J. & Correcher, V. (2000): Luminescence spectra of alkali feldspars: influence of crushing on the ultraviolet emission band. *Spectrosc. Lett.* **33**, 103-113.

Garcia-Guinea, J., Townsend, P.D., Sanchez-Muñoz, L. & Rojo, J.M. (1999): Ultraviolet-blue ionic luminescence of alkali feldspars from bulk and interfaces. *Phys. Chem. Minerals* **26**, 658-667.

Gorobets, B.S. & Rogojine, A.A. (2002): *Luminescent Spectra of Minerals*. Publ. RPC VIMS, Moscow, Russia.

Kraeff, A., Poorter, R.P.E. & Schuiling, R.D. (1980): Additional information on charoite. *Neues Jahrb. Mineral., Monatsh.*, 498-500.

McKeever, S.W.S. (1985): *Thermoluminescence of Solids*. Cambridge University Press, New York, N.Y.

Mitchell, R.H., Smith, C.B. & Vladykin, N.V. (1994): Isotopic composition of strontium and neodymium in potassic rocks of the Little Murun complex, Aldan Shield, Siberia. *Lithos* **32**, 243-248.

Nikishova, L.V., Lazebnik, Y.D. & Lazebnik, K.A. (1984): New data on charoite. *Acta Crystallogr.* **A40**, Suppl. C, 246.

Reguir, E. (2001): *Aspects of the Mineralogy of the Murun Alkaline Complex, Yakutia, Russia.* M.Sc. thesis, Lakehead Univ., Thunder Bay, Ontario, Canada.

Rogova, V.P., Rogov, Y.G., Drits, V.A. & Kuznetsova, N.N. (1978): Charoite, a new mineral, and a new jewellery stone. *Zap. Vses. Mineral. Obshchest.* **107**(1), 94-100 (in Russ.).

Rozhdestvenskaya, I.V. & Nikishova, L.V. (2002): Crystallochemical characteristics of alkali calcium silicates from charoitites. *Crystallogr. Rep.* **47**(4), 545-554.

Smith, G.S. & Snyder, R.L. (1979): F_N, a criterion for rating powder diffraction patterns and evaluating the reliability of powder indexing. *J. Appl. Crystallogr.* **12**, 60-65.

Vladykin, N.V. (2000): The Malyi Murun volcano-plutonic complex: an example of differentiated mantle magmas of lamproitic type. *Geochem. Int.* **38**, S73-S83 (Suppl. 1).

Yao, B.D., Shi, H.Z., Zhang, X.Y. & Zhang, L.D. (2001): Ultraviolet photoluminescence from nonbridging oxygen hole centers in porous silica. *Appl. Phys. Lett.* **78**(2), 174-176.

Received September 4, 2006, revised manuscript accepted September 27, 2008.